

Magnetic and electrical anisotropy with correlation and orbital effects in dimerized honeycomb ruthenate Li_2RuO_3

Seokhwan Yun^{1,2}, Ki Hoon Lee^{1,2}, Se Young Park^{1,2}, Teck-Yee Tan², Junghwan Park⁴,
Soonmin Kang^{1,2}, D. I. Khomskii⁵, Younjung Jo^{3*} and Je-Geun Park^{1,2*}

¹ *Department of Physics and Astronomy, Seoul National University, Seoul 08826, Korea*

² *Center for Correlated Electron System, Institute for Basic Science (IBS), Seoul 08826, Korea*

³ *Department of Physics, Kyungpook National University, Daegu 41566, Korea*

⁴ *Samsung SDI Co. Ltd., Yongin 17084, Korea*

⁵ *II. Physikalisches Institut, Universität zu Köln, 50937 Köln, Germany*

* **Corresponding Author:** jophy@knu.ac.kr & jgpark10@snu.ac.kr

Abstract

Li_2RuO_3 undergoes a structural transition at a relatively high temperature of 550 K with a distinct dimerization of Ru-Ru bonds on the otherwise isotropic honeycomb lattice. It exhibits a unique herringbone dimerization pattern with a largest ever reported value of the bond shrinkage of about ~ 0.5 Å. Despite extensive studies, both theoretical and experimental, however its origin and its effect on physical properties still remain to be understood. In this work, using high quality single crystals we investigated the anisotropy of resistivity (ρ) and magnetic susceptibility (χ) to find a very clear anisotropy: $\rho_{c^*} > \rho_b > \rho_a$ and $\chi_b > \chi_a > \chi_{c^*}$. For possible theoretical interpretations, we carried out density functional calculations to conclude that these anisotropic behavior is due to the correlation effects combined with the unique orbital structure and the dimerization of Ru $4d$ bands.

1. Introduction

How a certain pattern of bonds forms for the given lattices underlies the fundamental physics and/or chemistry of the materials concerned. The discovery by A. Kekulé of the resonating double-single carbon-carbon bonds for benzene is an outstanding case in point. A more modern example is the RVB (resonating valence bond) state proposed by P. Anderson as a ground state for a triangular lattice with $S=1/2$ [1]. Therefore, it is a fundamental, important question to ask why a particular bond differs from others, otherwise being equal. Another example is that of R. Peierls, who discovered an instability of phonon in one-dimensional lattice with one electron per ion, now known as Peierls theorem or sometimes just called as Peierls transition or dimerization[2]. As one goes to two-dimension or even three-dimension, the original argument of Peierls seems to become perhaps less relevant. However when aided with further help of other participants like an orbital degree of freedom, it becomes a little bit subtler[3]. There are several examples now, in which the orbital degree of freedom triggers certain dimerization to prevail over otherwise bonds of equal-distance, a notable example among Ru oxides being $\text{Ti}_2\text{Ru}_2\text{O}_7$ [4].

A_2MO_3 (A=Li or Na, M=transition metal elements) is a promising candidate in search for novel states originating from specific structural, electronic, and magnetic configurations with a honeycomb lattice. Many factors control the competition among Kitaev physics, magnetism, and dimerization for the honeycomb lattice, some of which include a number of transition metal d electrons, a strength of spin-orbit coupling, a strength of correlation effects, the Hund's rule coupling, and/or the ionic radii of the A-site element[5,6]. As the relevant energy scales become comparable to one another for $4d$ orbitals, the ground state of $4d$ transition metal oxides, in particular ruthenates, seem to be more delicate with the particular importance of the orbital degree of freedom[3,4,7]. One should also note that Ru has a moderate spin-orbit interaction of 75 meV as compared with either its $3d$ or $5d$ counterparts.

Honeycomb-lattice ruthenates, Li_2RuO_3 with four $4d$ electrons in the t_{2g} manifold, has attracted significant attention owing to the presence of an apparently orbital-selective Peierls transition (OSPT) leading to the strongest tendency toward dimerization among the known A_2MO_3 systems[8]. It undergoes a strong dimerized transition below a quite high transition temperature (~ 550 K); it also displays a surprisingly large overlap between orbitals of the

transition metal ions compared to other Li_2MO_3 structures[9]. Most interestingly, the dimerized bonds between Ru atoms exhibit a herringbone pattern with significant disproportionation between short and long bonds alternating along the bonding direction, and it changes a space group from $C2/m$ to $P2_1/m$. One has to note that the difference between the two bonds is as large as $\sim 0.5 \text{ \AA}$, which is the largest ever reported value of such bond shrinkage due to dimerization. In a way, it indicates that there exists a strong direct bonding between two neighboring Ru atoms. The local dimers of short Ru-Ru bonds show a structural long-range order and form a valence bond solid (VBS) with local spin singlet states[9,10,11]. In addition, at high temperature it exhibits a reduced local magnetic moment of $S = 1/2$, instead of $S = 1$ [11], which corresponds to a typical four $4d$ electron configuration. In order to explain the above properties, the dimer formation based on OSPT induced by orbital degeneracy was proposed[10, 12]. The electronic structure calculations showed that for each bond there is one pair of Ru $4d$ orbitals that can overlap directly through σ -bonding. The bond is then responsible for the formation of a dimer and exhibits a singlet character[9].

The directional orbital dependence is known to have larger effect in the case of edge- or face-sharing octahedron geometries than in a corner sharing geometry[3]. Ru electrons in the in-plane orbitals share oxygen octahedral edges and form strong σ -bonds with the bond strength comparable to the intra-atomic Hund's coupling energy. However, electrons in the orbitals that are orthogonal to the Ru_2O_2 dimer plane form weaker π and δ bonds. Thus, the electronic structure mainly from the π and δ bonds would be significantly affected by the local dimerization. For instance, the previous electronic structure calculations showed that for each bond there is one pair of Ru $4d$ orbitals that overlap directly through the σ bonding. The σ -bond is then subsequently responsible for the formation of dimer and exhibits a singlet state. It was expected that contributions from the bonds participating in the dimer would be smaller to the electrical and magnetic properties due to its strong binding energies. For instance, the electrons participating in the dimer bonds is located a few eV below the Fermi-level [11,12]. On the other hand, the electrons participating in the weaker bonds, which are located close to the Fermi-level, would more directly influence the physical properties of Li_2RuO_3 . In particular, the orbitals occupied by these latter electrons are degenerate owing to the lattice symmetry, in particular the nonsymmorphic symmetry of 2_1 , which somehow went unnoticed in the previous calculations. This degenerate band can be easily perturbed due to the considerable spin-orbit

coupling of Ru, forming a flat band; which itself is a very interesting observation.

It is worth noting that the electronic structures of Li_2RuO_3 are strongly modified near the Fermi-level due to several factors: the orbital degree of freedom, the correlation effects, the spin-orbit coupling, and the strong dimerization. As the energy scales of each of them are more or less comparable to one another, it becomes increasingly more important to assess carefully what aspect of the physical properties of Li_2RuO_3 is driven by any of them, in particular the trigonal distortion, the Coulomb U energy and the spin-orbit interaction. In order to address this question, we investigated the electrical and magnetic anisotropies using high-quality single crystals of Li_2RuO_3 . We also carried out DFT band calculations to assist interpreting the experimental results.

2. Experimental methods

Li_2RuO_3 single-crystals were synthesized using a self-flux growth method with Li_2CO_3 (99.995%, Alfa Aesar) and RuO_2 (99.95%, Alfa Aesar) as starting materials. In order to compensate for Li deficiency caused by difference in the evaporation pressure between Ru and Li and to achieve the correct stoichiometry[13,14], Li_2CO_3 and RuO_2 were mixed in a ratio of 1.08:1. The obtained mixture was placed in an alumina crucible and heated sequentially at 600, 900, and 1000 °C for 24 h at each of the dwelling temperatures. Then, it was pelletized and further subject to heat-treatment at 1100 °C for 48 h, which yielded shiny hexagonal crystals (a typical size of $\sim 200\text{ }\mu\text{m}$) as shown in the inset of Fig. 1a. The crystallinity and crystal axis of the obtained crystals were confirmed by X-ray diffraction (XRD) using Rigaku XtalLab P200 (Mo Target, averaged K_α) and Rietveld refinement using the WinPLOTER program[15].

Resistivity of the crystal was measured along the three principal crystallographic axes using the two-probe method due to the small size of the sample. The voltage applied between the two electrodes was kept below 100 mV in order to avoid any possible charging effects that could arise from the high mobility of the Li^+ ions[16]. We used two different set-ups for our resistivity measurements to cover a wide temperature range: one with a cryostat covering the

temperature range from 5 to 300 K and another one with a furnace covering the range from 300 to 650 K. For the magnetic susceptibility measurement, we co-aligned approximately 250 pieces of the crystals with a total mass of ~ 1.091 mg along the c^* -axis (perpendicular to the Ru honeycomb layer) using Kapton tape and stacked them in five layers (see the photo in the inset of Fig. 3a). The susceptibility measurement was then performed from room temperature down to 5 K, in an applied magnetic field of 1 T parallel to the c^* -axis and perpendicular to the a -axis, using a commercial magnetic property measurement system (MPMS3, Quantum Design).

Due to the small sample size of Li_2RuO_3 single-crystals and their sensitivity to sample misalignment, the magnetic anisotropy in the ab -plane was further evaluated using a torque magnetometer along the three main crystallographic axes. For this torque measurement, we mounted a single piece of Li_2RuO_3 single-crystal on top of a piezoresistive microcantilever and the torque due to the magnetization was measured through changes in the resistance of the piezomaterial with a Wheatstone bridge circuit (Fig. 3c). To measure the full anisotropy of the magnetic signals, we performed the measurements along θ_{c^*} with ϕ_{ba} -rotation: θ_{c^*} is the angle between the direction of the applied field and c^* -axis while ϕ_{ba} is the azimuthal angle in the ab -plane (see Fig. 3c). The direction of the magnetic field was controlled using a 9 T physical property measurement system (PPMS9, Quantum Design) and a rotator.

We also carried out the DFT calculations using WIEN2k[17] with $12 \times 6 \times 12$ k-points in a full Brillouin zone using TB-mBJ potential for exchange correlation[18,19]. We included the spin-orbit coupling in the calculations (spin-orbit coupling of Ru is about 75 meV). We also calculated the anisotropic resistivity with Wannier90[22,23] and susceptibility using the in-built options of WIEN2k.

3. Results

Figure 1a shows the Rietveld refinement of the single crystal X-ray diffraction results taken at room temperature. The number of peaks used for the refinement is approximately 1,700; the refined lattice parameters are $a = 4.931$ Å, $b = 8.795$ Å and $c = 5.132$ Å with the β angle of 108.22° at room temperature. The shortest Ru–Ru bond (red links in Fig. 1b) length (d_s) is

2.571 Å, while the lengths of the other bonds (orange links) are 3.048 Å (d_I) and 3.058 Å (d_L) (see Fig. 1b). We defined the measure of the dimerization strength as $(d_L - d_S)/d_S$, which becomes as large as 0.186: it is almost identical to the largest value reported from the previous results[9]. A passing note; from our extensive studies using both single crystals and powder samples we notice that this relative bond contraction defined above is a good measure of the quality of the samples.

Figure 2a shows the intensity of the (101) peak, one of the dimerization-related superlattice peaks, as a function of temperature up to 600 K. As one can see, it disappears dramatically above the transition temperature of approximately 550 K with a structural phase transition from $P2_1/m$ to $C2/m$. Figure 2b also shows the relative ratio of two lattice parameters b/a as a function of temperature. This ratio can also be used as a quick quality check of the sample; it decreases not only with excess Li, but also with Li defect[13,14]. For our sample, the ratio is found to be 1.784 at 300 K. Upon heating it converges to $\sqrt{3}$ at 600 K with a uniform inter Ru bond length[11], i.e. the honeycomb layer being composed of almost regular hexagons (inset in Fig. 2b).

In order to investigate the effects of both correlation and spin-orbit coupling on the dimerized state, we decided to examine the anisotropy of physical properties using single crystal samples: both Coulomb U correlation and the spin-orbit coupling are expected to induce nontrivial anisotropy in physical properties. First, the resistivity curves show the phase transition around 550 K with clear anisotropic behavior. For example, the c^* -axis resistivity is the largest over the whole temperature range probably because the honeycomb layer is separated by Li layers along this direction. Of particular note is an in-plane anisotropy: the b -axis resistivity is larger than the a -axis resistivity (Fig. 2c). This implies that an inter-dimer electronic hopping along the b -axis (d_I and d_S in Fig. 1b) becomes harder than that along the a -axis (d_L and d_S in Fig. 1b). The resistivity ratio ρ_b/ρ_a is determined to be ~ 2 above the phase transition, but it increases as the temperature decreases and becomes ~ 10 at 5 K. This strong in-plane anisotropy indicates directly strong directional hopping integrals, which are most likely due to the orbital degree of freedom of Ru $4d$ bands.

We also show an Arrhenius plot of the resistivity data in the inset of Fig. 2c. For all directions, the curves are well fitted with a straight line with an energy gap of approximately

0.15 eV in the high-temperature phase. However, surprisingly, they do not follow the activation formula in the low-temperature state with the herringbone patterned dimerized bonds and get even flatter than those above the phase transition temperature. In order to check whether this low-temperature flattening behavior is anything to do with possible topological insulating behavior as suggested for SmB_6 [20], we have used VASP2trace to examine the band topology and found that all the bands are topologically trivial in Li_2RuO_3 [24]. Thus, we believe that this low-temperature flattening behavior is more likely to be extrinsic, probably due to Li defects.

To examine this anisotropic behavior further, we carried out susceptibility measurement. The susceptibility curves shown in Fig. 3a are almost temperature-independent below the transition temperature due to the singlet formation of the Ru dimers. The typical up-turn behavior at low temperatures, most probably originating from paramagnetic impurities, is observed independent of the directions. But what is most remarkable is that the low-temperature susceptibility has a very large van Vleck paramagnetic contributions of $3 \sim 6 \times 10^{-4}$ emu/mol-Oe. We also note that the c^* -axis susceptibility is smaller than that along the in-plane direction. This tendency is consistent with the reported data at higher temperatures[21]. Due to the small sample size of Li_2RuO_3 single-crystals and sensitivity to sample misalignment, the in-plane anisotropy could not be quantitatively resolved with high accuracy using a SQUID magnetometer we used.

Therefore, we decided to use a torque magnetometer for more measurements. As shown in Fig. 3b and 3c, the magnetic easy axis can be uniquely identified from a complete angular dependence of the torque measurements, $\tau(\theta_{c^*})$. The orientation of the crystal on the lever, which was determined using X-ray measurements and crystal morphology, defines the plane of rotation in field. The amplitude of the $\sin 2\theta_{c^*}$ dependence is proportional to the principal components of magnetic anisotropy α_{ij} . Figure 3b shows that $\tau(\theta_{c^*})$ at different azimuthal angles ϕ_{ba} and $\tau(\theta_{c^*})$ can be fitted with a sinusoidal function with a period of π . At the same time, Figure 3c shows the fitted amplitude of the data with b -to- a rotation. Using these new data from the torque measurements, we find that the susceptibility in any in-plane direction is larger than the out-of-plane susceptibility. The difference between χ_{ab} and χ_{c^*} depends on the azimuthal angle; it is the largest along the b -axis and smallest along the a -axis. The ratio defined as $\alpha_{bc^*}/\alpha_{ac^*} = (\chi_b - \chi_{c^*})/(\chi_a - \chi_{c^*})$ is approximately 3.5 at 10 K. In addition,

$\chi_{ab}/\chi_{c*} = (\chi_a + \chi_b)/2\chi_{c*}$ is found to be approximately 1.36 at 10 K, consistent with the data obtained using the SQUID data in Figure 3a.

4. Discussion and analysis

In order to understand the observed anisotropic behavior in both resistivity and susceptibility, we carried out DFT calculations with the spin-orbit coupling (see Fig.4a). An important point worth noting is that when we used the standard potential (GGA or LDA) for our DFT calculation we could not open a band gap. Only when we used TB-mBJ potential, we succeeded in getting the indirect band gap of 170 meV. This band gap value is more or less consistent with the experimental values[13] although we must comment that the exact value of the band gap in the low-temperature phase is not yet accurately determined because of the experimental difficulties. This dependence on the potentials used for the DFT calculations effectively implicitly implies that the Coulomb U plays an important role, which is imbedded in the TB-mBJ potential. Of a further note, the metallic solution would not produce rightly the experimentally measured anisotropy in the physical properties. Thus, having the unique anisotropic behavior in both ρ and χ is a direct evidence of Coulomb U at work for Li_2RuO_3 .

Another point worth noting is the band degeneracy along some specific momentum directions: the Z-D and E-Z-C2-Y2 directions, as shown in Fig. 4a. Without the spin-orbit coupling, it is perfectly degenerate and becomes slightly split under the spin-orbit coupling of 75 meV. This degeneracy is protected by the nonsymmorphic symmetry of the low-temperature phase of $\text{P2}_1/\text{m}$. Interestingly, this degenerate and almost flat band gives rise to a large density of states just below the Fermi level: our Hall experiment shows that Li_2RuO_3 is intrinsically n -type. Thus, with some control of the Fermi level like gating experiments one may just be able to control the ground state, which is an interesting direction for future research.

With the band structures producing the correct value of the band gap, we then calculate both the resistivity and the susceptibility using the modules imbedded in the WIEN2k code. For example, the resistivity based on the band structure is calculated using semi-classical Boltzmann approach using Wannier90[22,23]. In this calculation, we could succeed in getting the correct anisotropy of out-of-plane and in-plane resistivity correct as one can see in Fig. 4b.

Interestingly, one can change this anisotropy by shifting the Fermi level by 0.1 eV with more electron doping. However, our calculations failed to produce the correct in-plane anisotropy of the resistivity. Experimentally, we found that the a-axis resistivity is smaller than the b-axis while our calculations produces the b-axis resistivity smaller than the a-axis. The origin of the discrepancy in the resistivity anisotropy is unclear at the moment. Our guess is that it may be due to the considerable band renormalization due the correlations effects. We have also calculated the susceptibility with the following values: $\chi_a = 1.83$, $\chi_b = 2.34$, and $\chi_c = 1.21$, all in units of 10^{-4} emu/mol Oe[25,26]. Remarkably, these calculations not only give the correct anisotropy, but give the values of the almost the same order of magnitude as experimentally found.

To summarize, we found a strong anisotropy in both resistivity and susceptibility data of single crystal Li_2RuO_3 . Using further theoretical studies, we verified that the anisotropy in the susceptibility is reproducible with the DFT calculations with the TB-mBJ potential, indicating the importance of the correlation effect.

Acknowledgements: We would like to thank Kisoo Park, Yukio Noda, Igor Mazin, Giniyat Khaliullin, and George Jackelli for useful discussion. Y. J. Jo was supported by National Research Foundation, Korea (NRF-2016R1A2B4016656, NRF-2018K2A9A1A06069211) and the work of D. Khomskii was funded by the Deutsche Forschungsgemeinschaft (DFG) - Project number 277146847 - CRC 1238. And the work at IBS CCES was supported by the Institute of Basic Science (IBS) in Korea (Grants No. IBS-R009-G1).

References

- [1] P. W. Anderson, Materials Research Bulletin 8, 153 (1973)
- [2] R. E. Peierls, Ann. Phys. Leipzig 4, 121 (1930)
- [3] D. I. Khomskii, Transition Metal Compounds (Cambridge Univ. Press, Cambridge, 2014)
- [4] S. Lee, J.-G. Park, D. T. Adroja, D. I. Khomskii, S. Streltsov, K. A. McEwen, H. Sakai, K. Yoshimura, V. I. Anisimov, D. Mori, R. Kanno and R. Ibberson, Nat. Mat. 5, 471 (2006)
- [5] Y. Singh, S. Manni, J. Reuther, T. Berlijn, R. Thomale, W. Ku, S. Trebst, and P. Gegenwart, Phys. Rev. Lett. 108, 127203 (2012)
- [6] H. Lei, W.-G. Yin, Z. Zhong and H. Hosono, Phys. Rev. B 89, 020409(R) (2014)
- [7] S. Kang, Y. Tseng, B. H. Kim, S. Yun, B. Sohn, B. Kim, D. McNally, E. Paris, C. H. Kim, C. Kim, T. W. Noh, S. Ishihara, T. Schmitt, and J.-G. Park, Phys. Rev. B 99, 045113 (2019)
- [8] Z. V. Pchelkina, A. L. Pitman, A. Moewes, E. Z. Kurmaev, T.-Y. Tan, D. C. Peets, J.-G. Park, and S. V. Streltsov, Phys. Rev. B 91, 115138 (2015)
- [9] Y. Miura, Y. Yasui, M. Sato, N. Igawa, and K. Kakurai, J. Phys. Soc. Jpn. 76, 033705 (2007)
- [10] G. Jackeli and D. I. Khomskii, Phys. Rev. Lett. 100, 147203 (2008)
- [11] S. A. J. Kimber, I. I. Mazin, J. Shen, H. O. Jeschke, S. V. Streltsov, D. N. Argyriou, R. Valentí, and D. I. Khomskii, Phys. Rev. B 89, 081408(R) (2014)
- [12] S. V. Streltsov and D. I. Khomskii, Phys. Rev. B 89, 16112(R) (2014)
- [13] J. Park, T.-Y. Tan, D. T. Adroja, A. Daoud-Aladine, S. Choi, D.-Y. Cho, S.-H. Lee, J. Kim, H. Sim, T. Morioka, H. Nojiri, V. V. Krishnamurthy, P. Manuel, M. R. Lees, S. V. Streltsov, D. I. Khomskii & J.-G. Park, Sci. Rep. 6, 25238 (2016)
- [14] M.-P. Jimenez-Segura, A. Ikeda, S. Yonezawa, and Y. Maeno, Phys. Rev. B 93, 075133 (2016)
- [15] J. Rodriguez-Carvajal, Physica B 192, 55 (1993)

- [16] M. Sathiya, G. Rousse, K. Ramesha, C. P. Laisa, H. Vezin, M. T. Sougrati, M-L. Doublet, D. Foix, D. Gonbeau, W. Walker, A. S. Prakash, M. Ben Hassine, L. Dupont and J-M. Tarascon, *Nat. Mater.* 6, 6276 (2013)
- [178] P. Blaha, K. Schwarz, G. Madsen, D. Kvasnicka, J. Luit, R. Laskowski, F. Tran and L. D. Marks, WIEN2k: an augmented plane wave + local orbitals program for calculating crystal properties (2001)
- [18] F. Tran and P. Blaha, *Phys. Rev. Lett.* 102, 226401 (2009)
- [19] A. D. Becke and E. R. Johnson, *J. Chem. Phys.* 124, 221101 (2006)
- [20] P. Syers, D. Kim, M. S. Fuhrer, and J. Paglione, *Phys. Rev. Lett.* 114, 096601 (2015)
- [21] K. Mehlawat and Y. Singh, *Phys. Rev. B* 95, 075105 (2017)
- [22] G. Pizzi, D. Volja, B. Kozinsky, M. Fornari, and N. Marzari, *Comp. Phys. Comm.* 185, 422 (2014)
- [23] A. A. Mostofi, J. R. Yates, G. Pizzi, Y.-S. Lee, I. Souza, D. Vanderbilt and N. Marzari, *Comput. Phys. Commun.* 185, 2309 (2014)
- [24] M.G. Vergniory, L. Elcoro, C. Felser, N. Regnault, B.A. Bernevig, Z. Wang, *Nature*, 566, 480 (2019)
- [25] F. Mauri and S. G. Louie, *Phys. Rev. Lett.* 76, 4246 (1996)
- [26] R. Laskowski and P. Blaha, *Phys. Rev. B* 85, 035132 (2012)

Figure captions

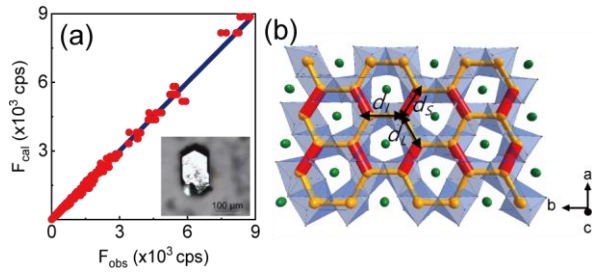


Fig. 1. (a) Rietveld refinement results of the Li_2RuO_3 single-crystal. The inset shows a typical hexagonal single-crystal. (b) Li_2RuO_3 at room temperature, viewed along the perpendicular direction to the Ru honeycomb layer in the ab -plane. The yellow and green spheres represent the Ru and Li ions, respectively. The blue polygons represent oxygen octahedrons. There are two unequal Ru–Ru bonds, i.e. dimerized bonds (red) and two other bonds (yellow) with similar lengths.

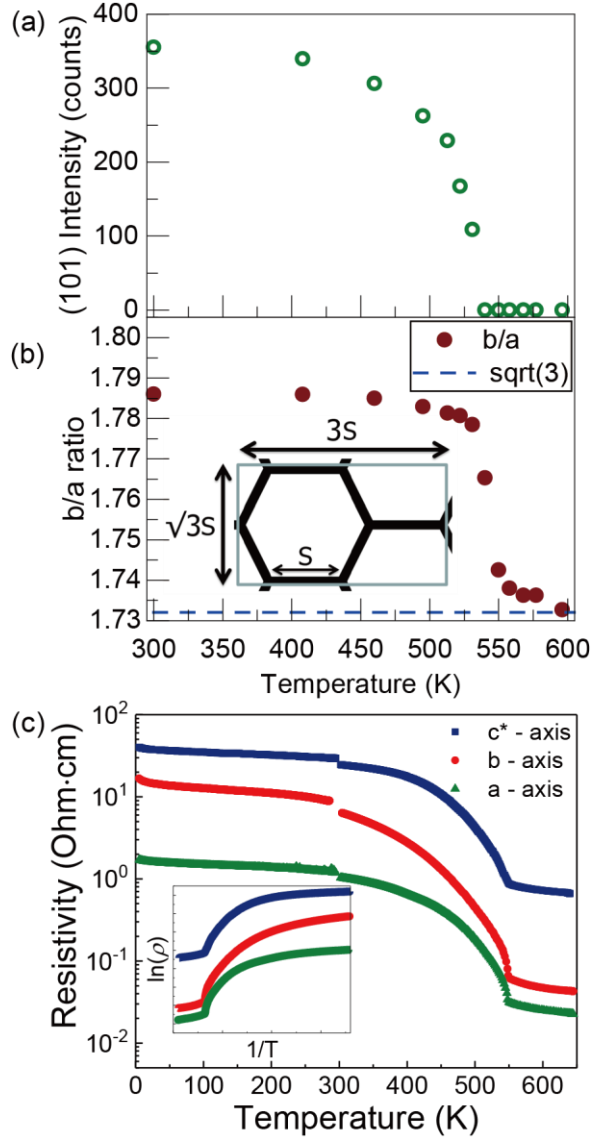


Fig. 2. Temperature dependence of (a) the intensity of the (101) peak and (b) the b/a ratio of the lattice parameters. The blue dashed line represents the value of $b/a \sim \sqrt{3}$, a value found for the honeycomb structure with an almost ideal honeycomb lattice. The inset shows an illustration of the ideal hexagonal honeycomb structure. (c) Resistivity of the Li_2RuO_3 single-crystal as a function of temperature T in the range of 5–650 K, along the a -(green), b -(red), and c^* -(blue) crystal axes. The inset shows the Arrhenius plots of the resistivity curves from 300 to 650 K.

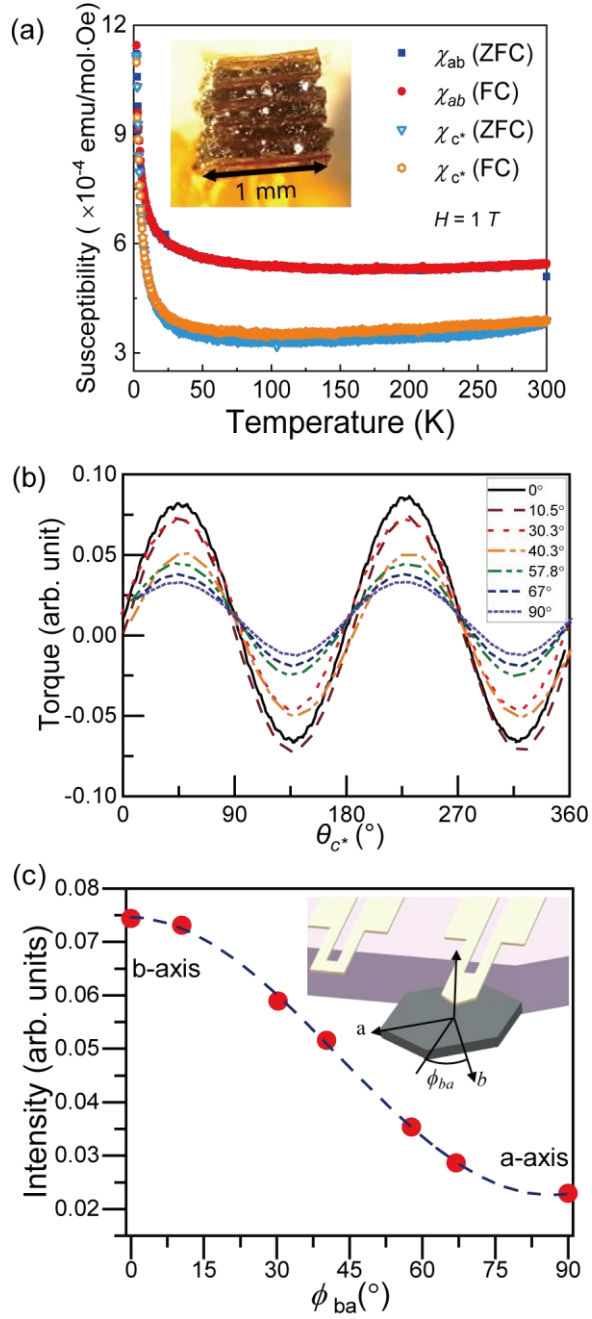


Fig. 3. (a) Susceptibilities of the c^* -axis-aligned single-crystals as a function of T in the range of 2–300 K, along the out-of-plane (χ_{c^*} , open marks) and in-plane (χ_{ab} , closed marks) directions; the inset shows the sample used for the measurement. (b) Angular-dependent torque measurement at fixed ϕ angles from $\phi_{ba} = 0^\circ$ (b -axis) to $\phi_{ba} = 90^\circ$ (a -axis). (c) Fitted amplitudes from the data with ab -rotation. The inset illustrates the crystal axes and rotating angles of the sample.

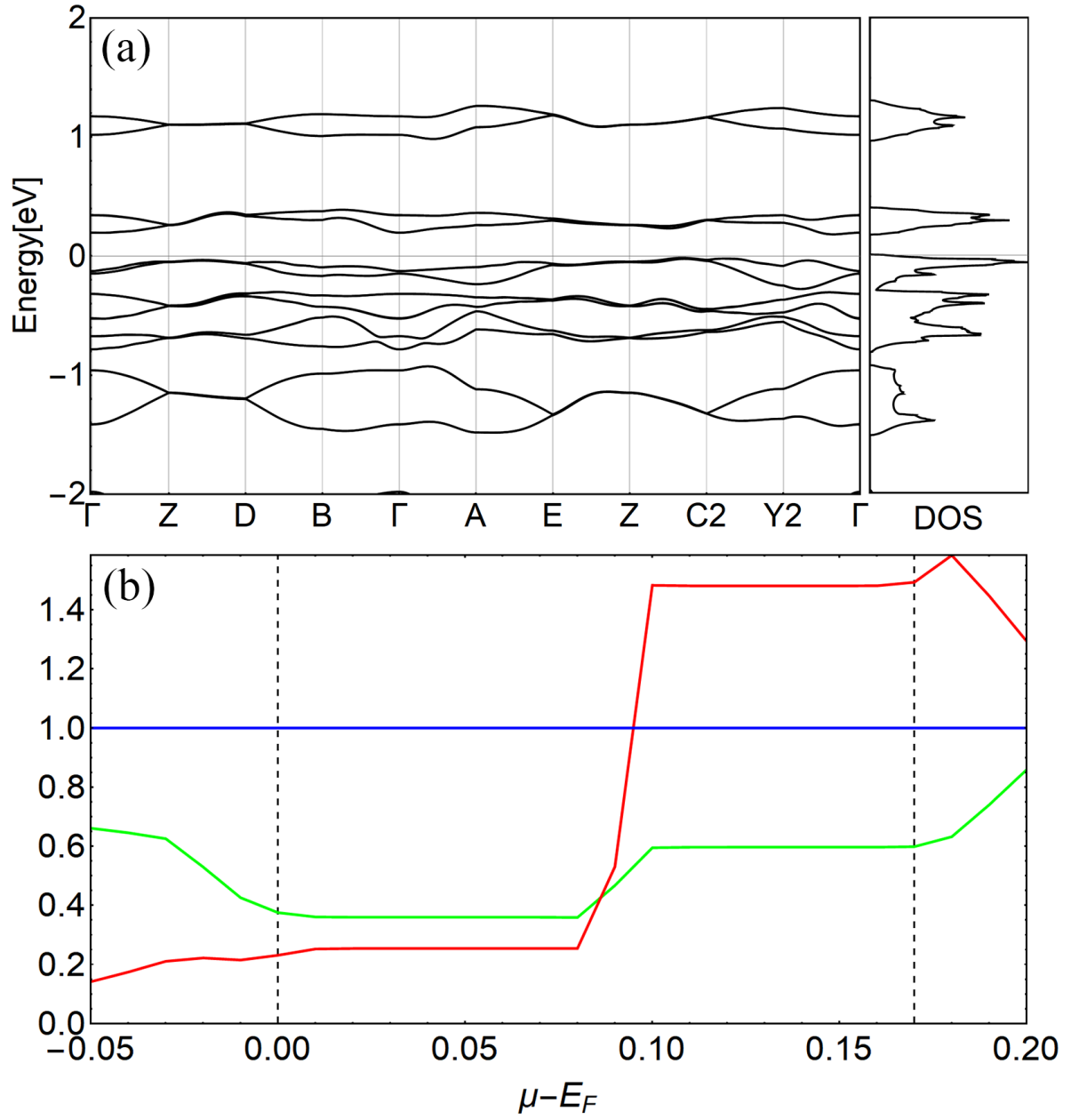


Fig. 4. (a) DFT band structure: Upper six bands are from anti-bonding states and lower six bands are from bonding states. (b) Resistivity divided by ρ_c^* at 100K with varying chemical potential. The green line is ρ_a/ρ_c^* and the red line is ρ_b/ρ_c^* .